

# A Compact Meander Line UHF RFID Antenna for Passive Tag Applications

Sudhir Bhaskar<sup>1, \*</sup> and Amit K. Singh<sup>2</sup>

**Abstract**—In this article, a meander line dipole antenna for radio frequency identification (RFID) tag is presented. The loaded meander antenna has a simple meander line structure with a spiral inductor at the end for size miniaturization, a  $T$ -match structure, and an inductively coupled parasitic element for impedance matching with the tag IC. The antenna is designed to operate in North American UHF RFID frequency band of 915 MHz. The size of the proposed tag antenna is  $50 \text{ mm} \times 12 \text{ mm}$  and has good impedance matching with Alien Higgs IC chip of  $13.5 - j111\Omega$  at the desired frequency band. The proposed tag antenna provides omnidirectional radiation pattern with a maximum read range of 3.5 m at an effective isotropic radiated power of 4 W. Simulation results are in good agreement with measurement results.

## 1. INTRODUCTION

Radio Frequency Identification (RFID) is a technique for automatic contactless identification of objects of interest by using radio frequency signals. RFID system has a number of applications, as in retail stores for stock management, in logistics supply chains for tracking of goods to reduce theft and loss of goods, in access control using college ID cards, E-passport for airport security, electronic toll payment for vehicles, ignition keys for anti-theft feature in high end cars, livestock identification and management in animal product industry, etc. [1]. Four different frequency bands are assigned for RFID applications; namely, LF (125–134 kHz), HF (13.56 MHz), UHF (840–960 MHz), and microwave (2.45 and 5.8 GHz). Among these frequency bands, UHF RFID systems are more attractive than others due to fast data transfer speed, more storage capability and higher reading range. Total UHF frequency band for RFID system is 840–960 MHz, but each country has allocated a specific frequency band for UHF RFID system: India (865–867 MHz), Australia (920–926 MHz), Taiwan (920–928 MHz), Japan (952–956 MHz), North America (902–928 MHz), Korea (908.5–910 MHz), Europe (865–868 MHz), China (920.5–924.5 MHz), Singapore (866–869 MHz and 923–925 MHz), etc. [2].

An RFID system consists of a tag and a reader. The reader transmits an interrogating radio frequency signal to the tags. This signal supplies power to the passive tags as well. The reader then receives a reply signal from the tag to complete the communication. A passive RFID tag is composed of an application specific integrated circuit (ASIC) and an antenna. There are two different working principles of RFID systems based upon the operating frequency. Low frequency and high frequency band RFID systems work on near-field coupling with load modulation principle [3], and UHF frequency band RFID system works on backscattered modulation in far field [4]. In near-field coupling, both reader and tag have coil antennas with power coupling between them based on transformer principle. In far field communication, the reader sends a modulated signal with unmodulated carrier pulses, which energizes the passive tag. When these unmodulated carrier pulses are converted to DC at the ends

---

Received 21 August 2020, Accepted 21 October 2020, Scheduled 30 November 2020

\* Corresponding author: Sudhir Bhaskar (sbhaskar.rs.ece@iitbhu.ac.in).

<sup>1</sup> Department of Electronics & Telecommunication Engineering, C V Raman Global University, Bhubaneswar, India. <sup>2</sup> Department of Electronics Engineering, Indian Institute of Technology (BHU) Varanasi, India.

of the tag antenna, a potential difference is developed across its terminals. The chip receives power from the antenna and replies back to the antenna by switching its input impedance between two states. One of them is the match state when the chip impedance is fully matched with the tag antenna. In this state, the chip is powered up. The other is a strongly mismatched state when the backscattering modulation takes place. Thus, the tag antenna is a crucial element because the overall performance of RFID system depends on the performance of it.

To date, a lot of RFID tag antenna structures have been proposed. A planar inverted-F antenna for the environment and platform tolerant tags is discussed in [5]. A spiral antenna with meander lines and loads is presented in [6] for passive UHF RFID transponders. It was optimized by using the guided artificial bee colony (GABC) algorithm. In [7], a fork-shaped tag antenna with two parasitic patches is presented. Parasitic patches allow the control of antenna input impedance. A CPW-fed folded-slot monopole antenna for the active RFID tags at 5.8 GHz is presented in [8]. Crossed-dipole compact circularly polarized antennas [9, 10] with a modified  $T$ -match network are reported with increased read distance. However, the overall size in circularly polarized case is more than linearly polarized antenna at the same operating frequency. In [11], a single sided dual antenna with an electromagnetic bandgap structure is proposed to enhance the gain. This is made of two antennas. One is for receiving energy and the other for backscattering. A dual-band antenna for high-frequency band and ultra high frequency band RFID systems based on the Hilbert-curve fractal is described in [12]. A hollowed-out meander dipole antenna [13] for printed RFID tags is developed in order to decrease ink consumption. Dual band functionality for Europe (867 MHz) and Japan (956 MHz) UHF RFID is obtained by using impedance perturbation method in a folded dipole antenna [14]. A two quarter-wave patch tag antenna with loop feed is presented in [15], in which low-cost feed loop and radiating antennas are designed separately. Among all these proposed designs, meander line antenna is the most suitable one for UHF RFID applications due to its miniaturized size, planar geometry, and omnidirectional radiation pattern.

This paper is a comprehensive report of [16] with detailed parametric study and more experimental results. In this article, a meander line antenna is proposed for 915 MHz UHF RFID tag applications. The antenna is symmetrical with respect to the origin and has a meander structure with spiral inductors at the ends, a  $T$ -match structure at the center, and an inductively coupled parasitic element above the meander structure. Meandering and spiral end loading is used for antenna size miniaturization. A  $T$ -match structure and an inductively coupled parasitic element is used for impedance matching between the antenna and tag IC. The combination of all these techniques in a single structure is studied in this work. The proposed meander line tag antenna has been designed and simulated by using Ansys high frequency structure simulator (HFSS) [17].

## 2. ANTENNA DESIGN

Figure 1 shows the proposed tag antenna configuration. The proposed antenna consists of four parts: a meander line dipole, spiral inductors at the ends, a  $T$ -match network, and a parasitic element. The antenna is fabricated with an FR4 glass epoxy substrate ( $\epsilon_r = 4.4$  and  $\tan \delta = 0.02$ ) of 1.6 mm height. The antenna is designed for Alien Higgs tag chip. The impedance of chip is frequency dependent, and at 915 MHz, it is  $13.5 - j111\Omega$ . The optimized values of proposed antenna parameters are described in Table 1.

Dipole antennas are popular among various tag antennas due to their simple structure, omnidirectional radiation pattern, and easy control of input impedance. However, the length of any dipole antenna at UHF band is 16.4 cm which is larger than the standard label dimensions. The combination of meandering and tip loading technique is used in the proposed antenna to make dipole antenna suitable for UHF RFID applications. Miniaturization of antenna size is done by using the meandering technique to fit the antenna within the standard label dimensions. A meander line dipole antenna (MDA) resonates at a lower frequency than a linear dipole antenna (LDA) of the same length [18]. Meandering not only reduces size of the antenna but also gets efficiency reduced because the currents in the adjacent vertical arms of any meander are in opposite directions, and they tend to cancel out each other. Therefore, instead of just meanders, spiral end loading is also used which reduces the overall size of an antenna without affecting the efficiency. A spiral conductor has much larger inductance than a meander line of the same size [19].

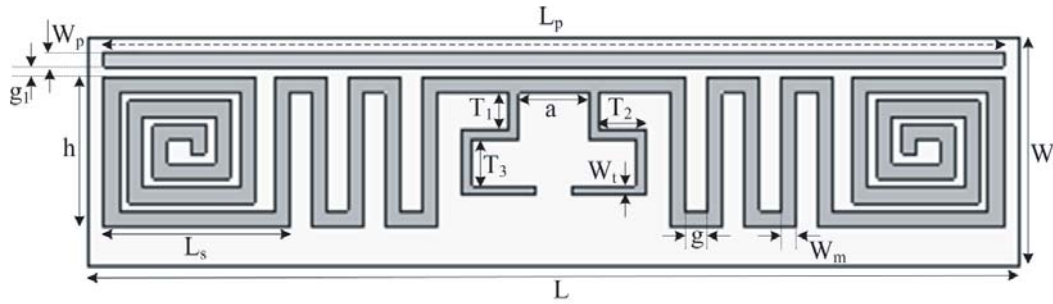


Figure 1. Configuration of the proposed antenna.

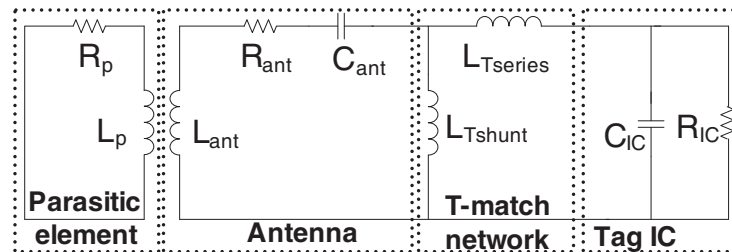


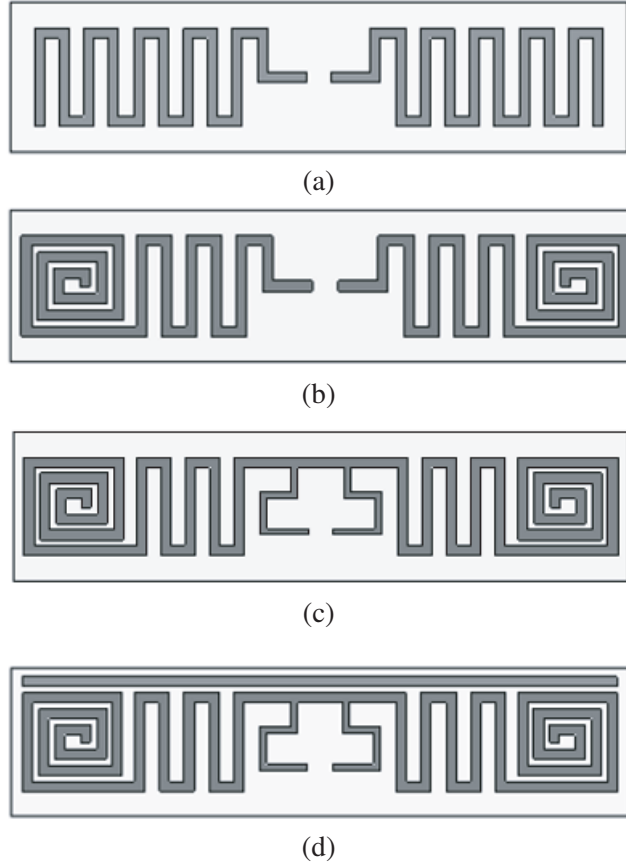
Figure 2. Equivalent RLC circuit model of the proposed structure.

Table 1. Optimized parameters of proposed antenna.

Parameter	Value (mm)	Parameter	Value (mm)
$L$	50	$L_s$	9.9
$W$	12	$T_1$	2
$L_p$	48.2	$T_2$	2.5
$W_p$	0.8	$T_3$	2.5
$W_m$	0.8	$W_t$	0.5
$g$	1	$a$	3.8
$g_1$	0.5	$h$	8

Figure 2 exhibits the equivalent RLC circuit model of the proposed structure to explain the impedance variation due to the  $T$ -match network and a parasitic element. The equivalent circuit can be divided into four parts in series in the following precise order: parasitic element, meander antenna,  $T$ -match network, and tag chip. The RFID chip has high capacitive impedance, so that for maximum power transfer, the antenna impedance should be highly inductive, and the complex conjugate of chip impedance by employing a  $T$ -match network and a parasitic element. At the center of the meandered structure, the  $T$ -match network is formed by connecting a dipole-like structure to enhance inductive reactance [20]. The  $T$ -match network provides series and shunt inductance as shown in Figure 2. By varying length and width of  $T$ -match network, the inductance of antenna can be varied without changing other antenna parameters. The impedance of the proposed antenna can be controlled by varying the different dimensional parameters of  $T$ -match ( $T_1, T_2, T_3, a, W_t$ ).

An inductively coupled parasitic loading bar of the same width as the meander structure is placed in close proximity of the latter, which produces mutual inductance by coupling between the two. The parasitic element is used for additional impedance matching between the antenna and microchip without modification in radiating element. The magnitude of mutual coupling and the added inductance are controlled by the length of parasitic element ( $L_p$ ) as well as the gap between parasitic element and



**Figure 3.** Evolution steps of proposed antenna, (a) meander line antenna, (b) meander line with end spiral antenna, (c) Meander line with end spiral and  $T$ -match network, (d) Proposed antenna.

meandered section ( $g_1$ ) [21, 22].

The further effects of spiral end structure,  $T$ -match network, and parasitic element on characteristics of the meander line antenna are now investigated. The four steps of evolution of the proposed antenna are depicted in Figures 3(a)–(d). The overall substrate dimension ( $L \times W$ ) and meander line strip width  $W_m$  remain the same in all steps. For the miniaturized antenna design at UHF band, a meandered dipole is used instead of a linear dipole as shown in Figure 3(a), and this structure resonates at 4 GHz. In Figure 3(b), the ends of meander section are replaced by spiral resonators, thus, enabling the antenna to resonate at 3.4 GHz as shown in Figure 4. Figure 3(c) shows the meandered line end spiral antenna with a  $T$ -match network making the structure to resonate at a further lower frequency (1.08 GHz). Figure 3(d) shows the final structure with an inductively coupled parasitic element rendering the antenna to resonate at the desired frequency of 915 MHz. The simulated return losses of all four cases are shown in Figure 4.

### 3. PARAMETRIC ANALYSIS

Each geometrical parameter has a different effect on input impedance and the reflection coefficient of proposed antenna. Parametric analysis has been carried out by varying one parameter at a time when keeping all the other parameters constant. The effects of variation of meander line height ( $h$ ), gap between meander line and the parasitic element ( $g_1$ ), spacing of meander element ( $g$ ),  $T$ -match network width ( $W_t$ ) on input impedance, and reflection coefficient are investigated. The impact of changing  $T$ -match parameters ( $T_1$ ,  $T_2$ ,  $T_3$ ,  $a$ ) on antenna input impedance is also investigated to understand the controlling of antenna input impedance by  $T$ -match network.

In order to analyze the effect of the spacing of meander element ( $g$ ) on input impedance and

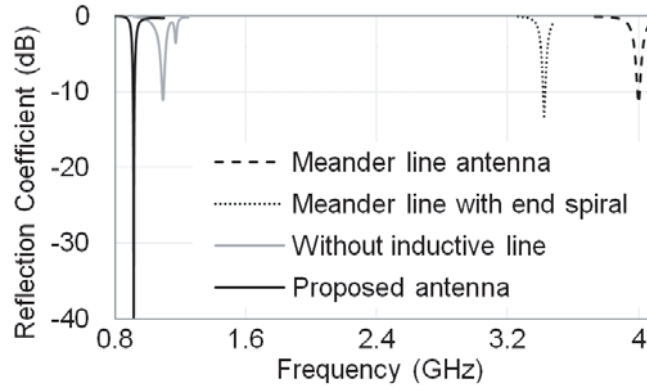


**Figure 4.** Simulated reflection coefficient versus frequency characteristics.

reflection coefficient, the antenna is simulated by varying parameter ( $g$ ) from 0.9 mm to 1.1 mm while keeping other parameters constant ( $W_t = 0.5$  mm,  $h = 4$  mm,  $g_1 = 0.5$  mm). It is observed from Figure 5(a) that the imaginary impedance of the antenna at 915 MHz remains constant, and the real part of input impedance increases with increment in parameter ( $g$ ). The real part of input impedance can be changed by varying parameter  $g$ . Figure 5(b) shows the effect of variation in  $g$  on reflection coefficient of the antenna. The value of  $g$  for optimum reflection coefficient is 1 mm.

To examine the effect of width of  $T$ -match network ( $W_t$ ) on the performance of the antenna,  $W_t$  is varied from 0.4 mm to 0.6 mm while the other parameters are kept constant ( $g = 1$  mm,  $h = 4$  mm,

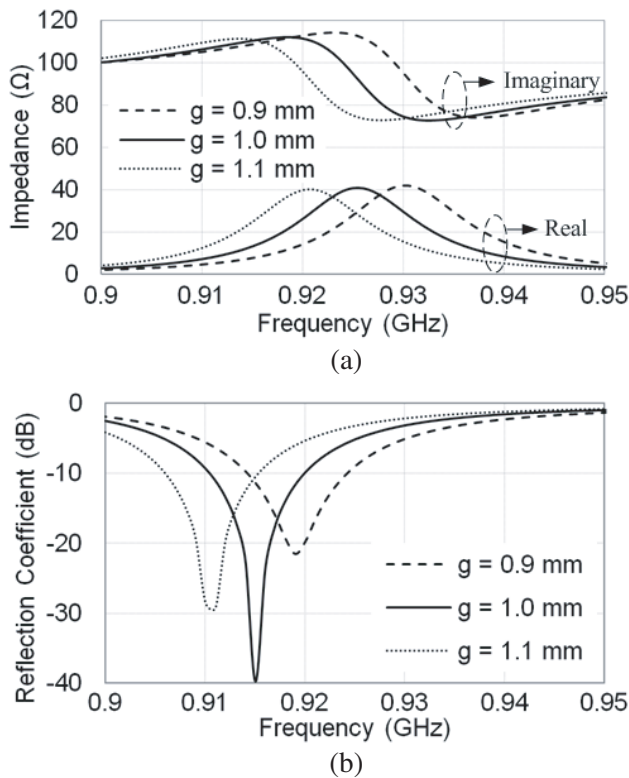


**Figure 5.** (a) Impedance and (b) Reflection coefficient for different values of the spacing of meander element  $g$ .

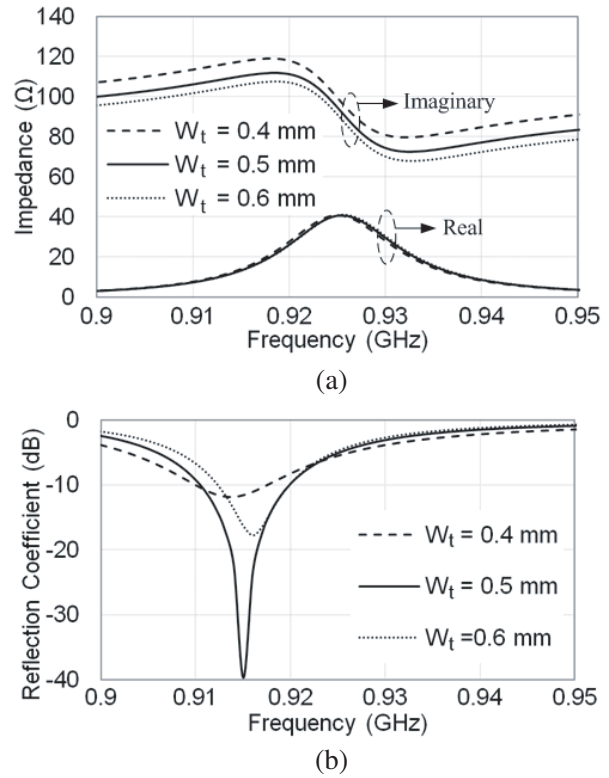


**Figure 6.** (a) Input impedance and (b) Reflection coefficient for different values of  $T$ -match network width  $W_t$ .

$g_1 = 0.5$  mm). From Figure 6, it is realized that resonating frequency is less sensitive to variation in parameter  $W_t$ , but it has a great influence on impedance matching between the antenna and IC. The imaginary part of input impedance of antenna decreases with increase in  $W_t$  whereas the real part of input impedance remains the same. The imaginary part of input impedance of antenna can be varied by altering the width of  $T$ -match network ( $W_t$ ). Antenna impedance matching is obtained with IC at  $W_t = 0.5$  mm during variation of width of  $T$ -match network ( $W_t$ ).

Figure 7 exhibits the effect of variation in meander line height ( $h$ ) on input impedance and reflection coefficient of the proposed antenna while keeping other parameters constant ( $g = 1$  mm,  $W_t = 0.5$  mm,  $g_1 = 0.5$  mm). Both real and imaginary parts of input impedance vary with variation in parameter  $h$ , and the resonant frequency shifts towards lower frequency with an increase in meander line height ( $h$ ). This phenomenon occurs because the overall length of meander line antenna increases with increase in  $h$ . At the optimized meander line height  $h = 4$  mm, resonance is at 915 MHz.

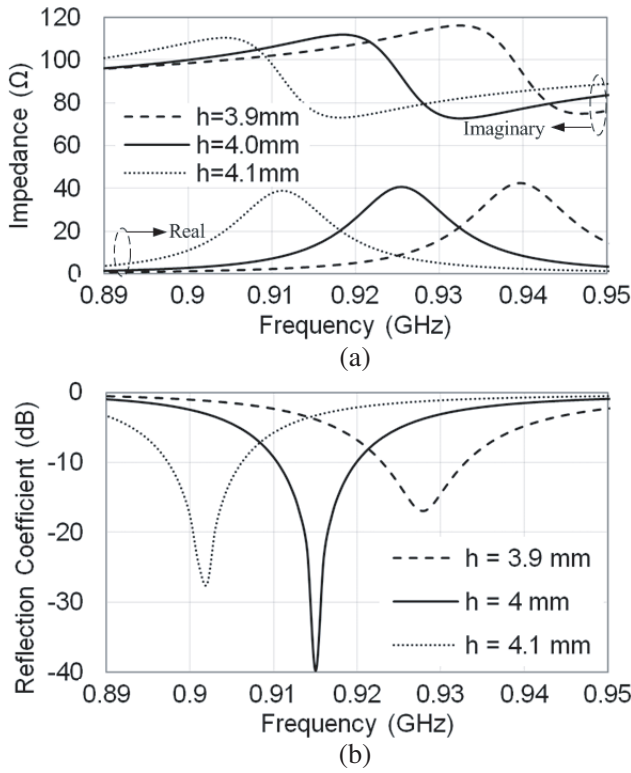


**Figure 7.** (a) Input impedance and (b) Reflection coefficient for different values of meander line height  $h$ .

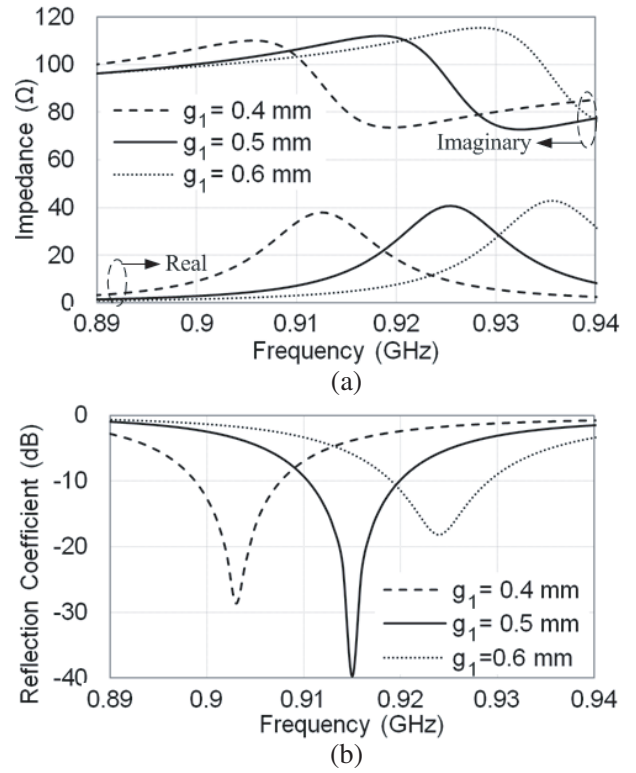


**Figure 8.** (a) Impedance and (b) Reflection coefficient for different values of gap between meander line and parasitic element  $g_1$ .

Figure 8(a) depicts the simulated real and imaginary parts of input impedance of the proposed structure with frequency for the different values of gap  $g_1$  between meander line and parasitic element while keeping other parameters constant ( $g = 1$  mm,  $W_t = 0.5$  mm,  $h = 4$  mm). Both real and imaginary parts of input impedance are sensitive to coupling distance between meander line and the parasitic element. The variation of reflection coefficient with frequency is plotted in Figure 8(b). It is noticed that the resonant frequency of antenna shifts towards higher frequency with increase in  $g_1$  by keeping other parameters constant. The optimized value of parameter  $g_1$  is found to be 0.5 mm. It is observed from the parametric study that with the optimized values of the above parameters, input impedance of the antenna is  $13.31 + j110.20\Omega$  for 915 MHz, which is approximately the complex conjugate of the tag-chip impedance.

### 4. RESULTS AND DISCUSSIONS

The fabricated antenna prototype is shown in Figure 9. As the proposed meander line antenna is a balanced dipole type antenna, therefore, its input impedance and return loss characteristics with frequency cannot be measured directly by using only single ended two-port vector network analyzer because VNAs are terminated by using unbalanced ports like coaxial port. When a balanced RFID tag antenna is connected to an unbalanced port, unequal currents flow in the terminals of the antenna, making an accurate measurement of the impedance of balanced antenna very difficult.

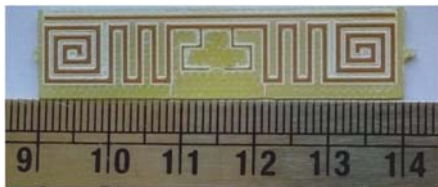


**Figure 9.** A fabricated prototype of the proposed tag antenna.

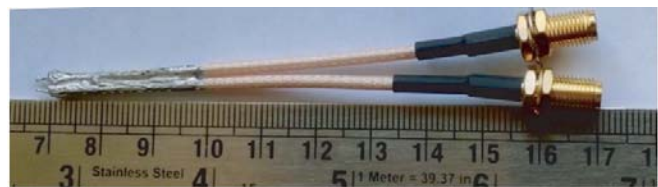


**Figure 10.** Semi-rigid differential probe test fixture.

Balun method [23], mirror image method [24], and differential probe method [25] are the most common methods for the input impedance measurement of an RFID tag antenna. Balun is a balanced to unbalanced converter that provides differential currents at end port. In the mirror image method, half part of the symmetric antenna is placed over a large conducting ground plane, and the input impedance of this half part of the antenna structure is measured by using a network analyzer. The complex input impedance of the full antenna is twice of the measured impedance of half antenna. In this work, differential probe method is used for measurement. A differential probe test fixture is made of two semi-rigid coaxial cables which are soldered together on the outer conductor as shown in Figure 10. One end of the differential probe has small extended inner connectors that are connected to the antenna under test, and the other end of the test fixture is connected to a VNA with cables. The errors introduced by the test fixture in the measurement of parameters are taken care of by adopting port extension technique as shown in Figure 11(a).

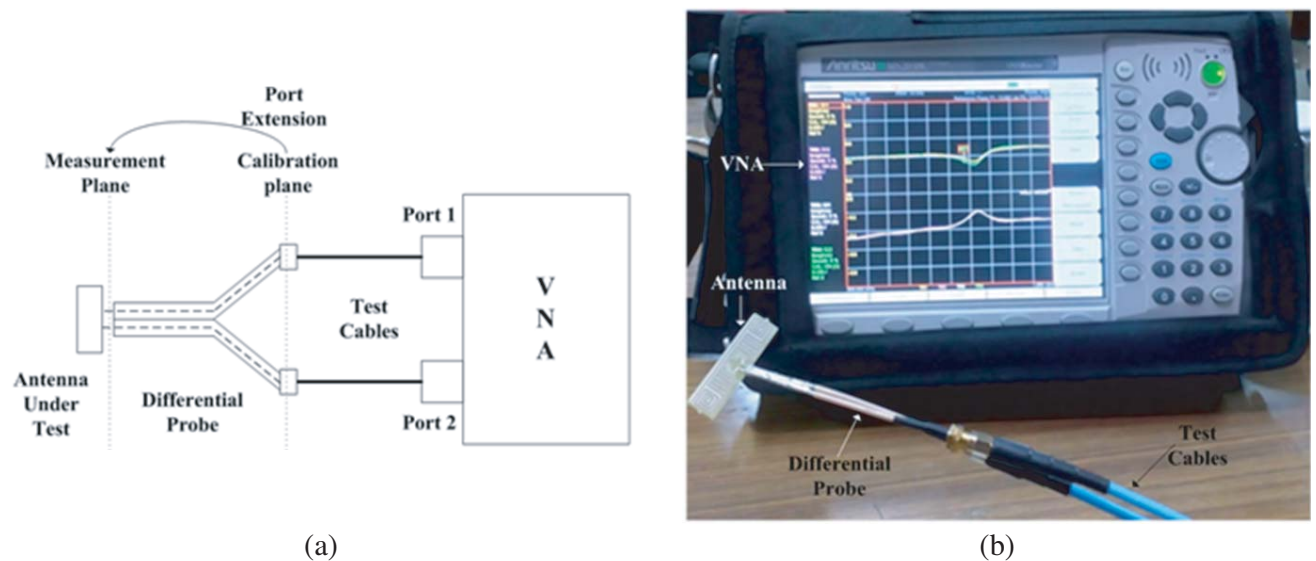


**Figure 11.** (a) Schematic configuration of measurement setup with differential probe, (b) impedance measurement setup with VNA.

The  $S$ -parameters of proposed antenna are measured, and then by using conversion formulas [26] the differential input impedance ( $Z_d$ ) of tag antenna is calculated:

$$Z_d = \frac{2Z_0(1 - S_{11}S_{22} + S_{12}S_{21} - S_{12} - S_{21})}{(1 - S_{11})(1 - S_{22}) - (S_{21}S_{12})} \quad (1)$$

The proposed antenna is symmetrically balanced, thus Equation (1) can be modified by having  $S_{11} = S_{22}$  and  $S_{21} = S_{12}$ :

$$Z_d = \frac{2Z_0(1 - S_{11}^2 + S_{12}^2 - 2S_{12})}{(1 - S_{11})^2 - S_{12}^2} \quad (2)$$

Figure 12 shows measured and simulated real and imaginary parts of the input impedance of the antenna. The measured input impedance at 915 MHz is  $15.55 + j111.4\Omega$ , while that obtained by simulation is  $13.311 + j110.201\Omega$  which is approximate to the complex conjugate of chip impedance. Power reflection coefficient of the proposed antenna is calculated using input impedance and is plotted in Figure 13. The fabricated antenna resonates at 913 MHz. There is little incongruence between the measured and simulated power reflection coefficient results which can be attributed to fabrication imperfections and port extension errors of the differential probe.

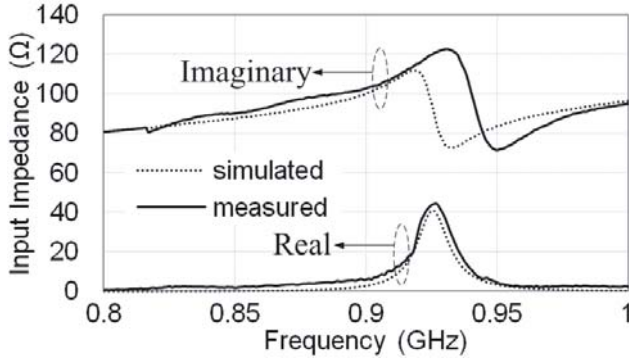


**Figure 12.** Measured and simulated real part and imaginary part of input impedance of the proposed antenna.

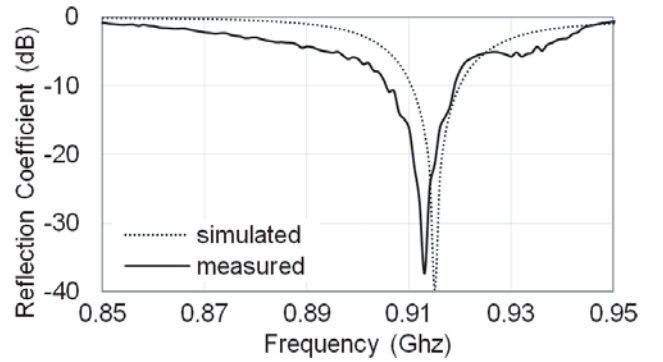


**Figure 13.** Measured and simulated reflection coefficient variation of the proposed antenna.

Figure 14 exhibits the radiation pattern of the meandered antenna at 915 MHz in both  $E$ -plane and  $H$ -plane. The antenna has omnidirectional radiation pattern identical to that by a dipole antenna which is desired for RFID applications.

Read range is an important performance characteristic of an RFID system. Read range is the maximum possible communication gap between reader and tag, i.e., the maximum distance at which the reader can detect the tag. Read range depends on many factors like impedance matching between tag antenna and IC, antenna gain, communication environment, tag orientation, and platform material on which tag is connected. Maximum read range  $r_{\max}$  can be determined as follows [27]

$$r_{\max} = \frac{\lambda}{4\pi} \sqrt{\frac{P_r G_r G_t (1 - |\Gamma|^2)}{P_{th}}} \quad (3)$$

and  $\Gamma = \frac{Z_c - Z_a^*}{Z_c + Z_a}$ , where  $r$  is the reflection coefficient, and  $\tau$  is the power transmission coefficient

$$\tau = \frac{4R_c R_a}{|Z_c + Z_a|^2}, \quad 0 \leq \tau \leq 1$$

$Z_c$  and  $Z_a$  are the chip and antenna impedance, respectively.  $\lambda$  is the operating wavelength.  $P_r$  and  $g_r$  are the power radiated and gain of the reader antenna, respectively. The product of  $P_r$  and  $g_r$  is

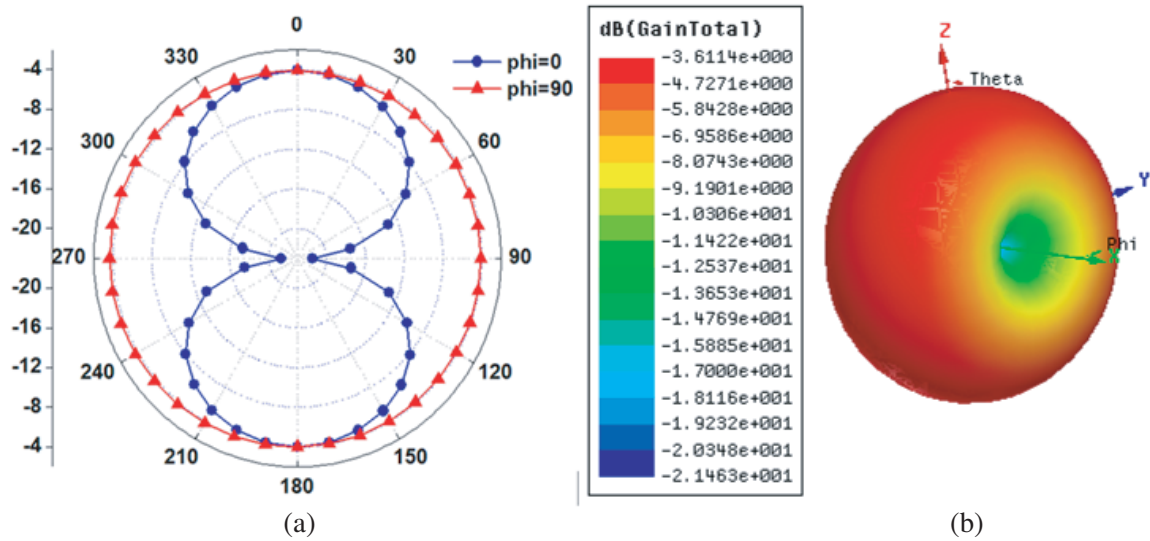


**Figure 14.** Simulated far-field radiation pattern at 915 MHz (a) *E*-plane and *H*-plane, (b) 3D polar plot.

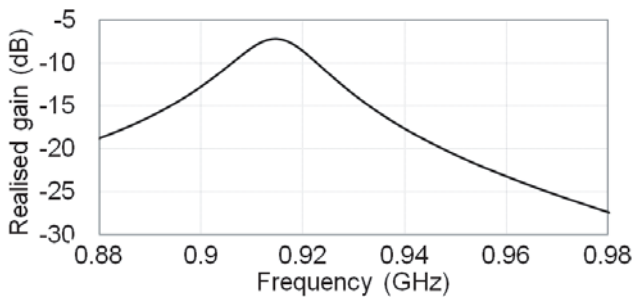


**Figure 15.** Simulated gain of the proposed antenna.

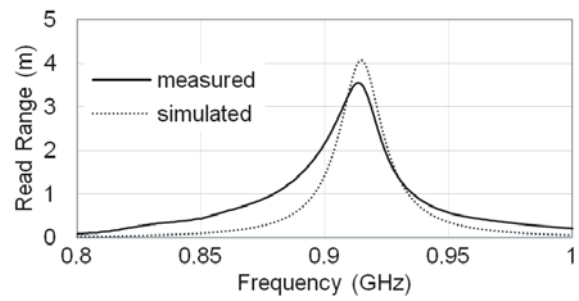


**Figure 16.** Measured and simulated read range of the antenna.

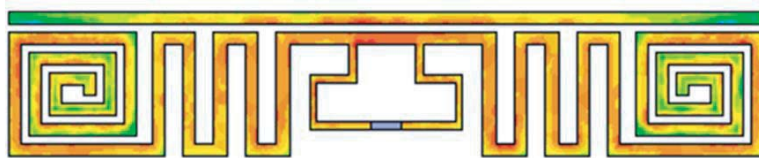


**Figure 17.** Simulated surface current density of the designed antenna at 915 MHz.

called EIRP (Effective Isotropic radiated power), which is regulated at 4 watts in accordance with FCC (Federal Communication Commission).  $g_t$  is the gain of tag antenna that is shown in Figure 15.  $P_{th}$  is the threshold power, i.e., the minimum required power to energize the tag chip. The proposed antenna is designed for Alien Higgs IC chip (threshold power  $P_{th} = -14$  dBm). The result for read range with different frequencies is shown in Figure 16 for values of EIRP = 4 W and  $P_{th} = -14$  dBm. At 915 MHz, the peak simulated read range is 4.06 m, and measured read range is 3.5 m. The simulated surface current distribution of the designed antenna is exhibited in Figure 17. A high current density in and near the matching loop is observed.

Table 2 summarizes the comparison among the proposed antenna and many of those reported previously in literature in terms of read range, frequencies of operation, and dimension. All the compared antennas are designed to operate in a single band except [14]. It is identified that the proposed antenna

**Table 2.** Performance Comparison of the proposed antenna with those in the literature.

Antenna	Read range (m)	Dimension (mm <sup>2</sup> )	Frequencies of operation (MHz)	% Reduction in size
[5]	1.4–2.2	76.6 × 60.2	895–924	86.98
[7]	3.8–4.3	120 × 30	899–932	83.33
[11]	4.4	50 × 67	925	82.09
[14]	3.3–5	66 × 20	865–868, 950–956	54.54
[15]	0.5–3	80 × 25	900–930	70
[21]	6.3	17.96 × 35.6	910–919	6.15
[22]	5	96 × 17	866–869	63.23
Proposed Antenna	3.5	50 × 12	905–919	-

has a miniaturized dimension. The read range of the proposed antenna tends to be smaller than some of the previously reported antennas on account of the fact that the reported antennas are designed for different tag IC, and the read range of a tag depends not only on the antenna but also on the tag IC as shown in Equation (3). Otherwise, the read range of the proposed antenna is comparable with the same tag IC antennas [7, 11, 15].

## 5. CONCLUSION

In this work, a meander line dipole antenna has been developed and measured for 915 MHz UHF RFID applications. The designed antenna consists of a  $T$ -match network, an inductively coupled parasitic element, and a spiral structure for good conjugate impedance matching with tag IC and size miniaturization. This meander antenna provides comparable read range with a smaller size than same IC UHF RFID tag antennas. The maximum read range of proposed antenna with Alien Higgs tag IC chip is 3.5 m. Measured and simulated read ranges are in good agreement. The antenna has an omnidirectional radiation pattern which makes it suitable for UHF band RFID applications.

## REFERENCES

1. Paret, D., *RFID at Ultra and Super High Frequencies: Theory and Application*, John Wiley & Sons, 2009.
2. Finkenzerler, K., *RFID Handbook: Radio-Frequency Identification Fundamentals and Applications*, Wiley, New York, 2004.
3. Heidrich, J., D. Brenk, J. Essel, G. Fischer, R. Weigel, E. Nuremberg, S. Schwarzer, and K. Seemann, "The roots, rules, and rise of RFID," *IEEE Microwave Magazine*, Vol. 11, 78–86, May 2010.
4. Loo, C.-H., K. Elmahgoub, F. Yang, A. Elsherbeni, D. Kajfez, A. Kishk, and T. Elsherbeni, "Chip impedance matching for UHF RFID tag antenna design," *Progress In Electromagnetics Research*, Vol. 81, 359–370, 2008.
5. Cho, C., H. Choo, and I. Park, "Printed symmetric inverted-F antenna with a quasi-isotropic radiation pattern," *Microwave and Optical Technology Letters*, Vol. 50, 927–930, April 2008.
6. Goudos, S. K., K. Siakavara, A. Theopoulos, E. E. Vatiadis, and J. N. Sahalos, "Application of Gbest-guided artificial bee colony algorithm to passive UHF RFID tag design," *International Journal of Microwave and Wireless Technologies*, Vol. 8, 537–545, May 2016.
7. Kim, K. H., J. G. Song, D. H. Kim, H. S. Hu, and J. H. Park, "Fork-shaped RFID tag antenna mountable on metallic surfaces," *Electronics Letters*, Vol. 43, 1400–1402, December 2007.
8. Bhaskar, S., S. Singhal, and A. K. Singh, "Folded-slot active tag antenna for 5.8 GHz RFID applications," *Progress In Electromagnetics Research C*, Vol. 82, 89–97, March 2018.

9. Bhaskar, S. and A. K. Singh, "Linearly tapered meander line cross dipole circularly polarized antenna for UHF RFID tag applications," *International Journal of RF and Microwave Computer-aided Engineering*, e21563, 2018.
10. Tran, H. H., S. X. Ta, and I. Park, "A compact circularly polarized crossed-dipole antenna for an RFID tag," *IEEE Antennas and Wireless Propagation Letter*, Vol. 14, 674–677, March 2015.
11. Kamalvand, P., G. K. Pandey, and M. K. Meshram, "A single-sided meandered-dual-antenna structure for UHF RFID tags," *International Journal of Microwave and Wireless Technologies*, Vol. 9, 1419–1426, July 2017.
12. Kenari, M. A., M. N. Moghadasi, R. A. Sadeghzadeh, B. S. Virdee, and E. Limiti, "Dual-band RFID tag antenna based on the Hilbert-curve fractal for HF and UHF applications," *IET Circuits, Devices & Systems*, Vol. 10, 140–146, 2016.
13. Marindra, M. J., P. Pongpaibool, W. Wallada, and S. Siwamogsatham, "An optimized ink-reducing hollowed-out arm meander dipole antenna structure for printed RFID tags," *International Journal of Microwave and Wireless Technologies*, Vol. 9, 469–479, March 2017.
14. Barman B., S. Bhaskar, and A. K. Singh, "Spiral resonator loaded S-shaped folded dipole dual band UHF RFID tag antenna," *Microwave and Optical Technology Letters*, 1–7, 2018.
15. Yang, P. H., Y. Li, L. Jiang, W. C. Chew, and T. T. Ye, "Compact metallic RFID tag antennas with a loop-fed method," *IEEE Transactions on Antennas and Propagation*, Vol. 59, 4454–4462, December 2011.
16. Bhaskar, S. and A. K. Singh, "Meander line tag antenna with inductively coupled parasitic element and T-loop feed," *International Symposium on Antennas and Propagation (ISAP)*, Phuket, 2017.
17. Ansoft Corporation, HFSS, High frequency structure simulator version11, Finite element package, Ansoft Corporation, Available at:<http://www.ansoft.com>.
18. Marrocco, G., "The art of UHF RFID antenna design: impedance-matching and size-reduction techniques," *IEEE Antennas Propagation Magazine*, Vol. 50, 66–79, February 2008.
19. Deavours, D., and D. Dobkin, *UHF passive RFID tag antennas, Microstrip and Printed Antennas: New Trends, Techniques and Applications*, 263–303, Wiley, 2010.
20. Zamora, G., S. Zuffanelli, F. Paredes, F. Martin, and J. Bonache, "Design and synthesis methodology for UHF-RFID tags based on the *T*-match network," *IEEE Transactions on Microwave Theory and Techniques*, Vol. 61, 4090–4098, December 2013.
21. Kim, T., U. Kim, and J. Choi, "Design of a compact UHF RFID tag antenna using an inductively coupled parasitic element," *Microwave and Optical Technology Letters*, Vol. 53, 239–242, February 2011.
22. Rao, K. V. S., P. V. Nikitin, and S. F. Lam, "Antenna design for UHF RFID tags: a review and a practical application," *IEEE Transactions on Antennas and Propagation*, Vol. 53, 3870–3876, December 2005.
23. Wang, B., Y. Zhuang, X. Li, X. Ren, Z. Qi, and Y. Zhang, "A novel method for impedance measurement of balanced UHF RFID tag antennas," *Journal of Electromagnetic Waves and Applications*, Vol. 28, 2059–2066, February 2014.
24. Tikhov, Y., I. J. Song, and Y. H. Min, "Compact ultrahigh-frequency antenna designs for low-cost passive radio frequency identification transponders," *IET Microwaves, Antennas & Propagation*, Vol. 1, 992–997, October 2007.
25. Kuo, S.-K., S.-L. Chen, and C.-T. Lin, "An accurate method for impedance measurement of RFID tag antenna," *Progress In Electromagnetics Research*, Vol. 83, 93–106, 2008.
26. Qing, X., C. K. Goh, and Z. N. Chen, "Impedance characterization of RFID tag antennas and application in tag co-design," *IEEE Transactions Microwave Theory Techniques*, Vol. 57, 1268–1274, May 2009.
27. Paredes, F., G. Zamora, S. Zuffanelli, F. J. Herraiz-Martinez, F. Martin, and J. Bonache, "Free-space and on-metal dual-band tag for UHF-RFID applications in Europe and USA," *Progress In Electromagnetics Research*, Vol. 141, 577–590, 2013.